Thermally Induced Fluid Reversed Hexagonal (H_{II}) Mesophase

Idit Amar-Yuli,[†] Ellen Wachtel,[‡] Deborah E. Shalev,[§] Hagai Moshe,[†] Abraham Aserin,[†] and Nissim Garti*[,†]

Casali Institute of Applied Chemistry, The Institute of Chemistry, and Wolfson Centre for Applied Structural Biology, The Hebrew University of Jerusalem, Jerusalem 91904, Israel, and Faculty of Chemistry, The Weizmann Institute of Science, Rehovot 76100, Israel

Received: August 19, 2007; In Final Form: September 20, 2007

In the present study we characterized the microstructures of the L_c and H_{II} phases in a glycerol monooleate (GMO)/tricaprylin (TAG)/water mixture as a function of temperature. We studied the factors that govern the formation of a low-viscosity H_{II} phase at relatively elevated temperatures (>35 °C). This phase has very valuable physical characteristics and properties. The techniques used were differential scanning calorimetry (DSC), wide- and small-angle X-ray scattering (WAXS and SAXS, respectively), NMR (self-diffusion and ^{2}H NMR), and Fourier transform infrared **(**FTIR) spectroscopies. The reverse hexagonal phase exhibited relatively rapid flow of water in the inner channels within the densely packed cylindrical aggregates of GMO with TAG molecules located in the interstices. The existence of two water diffusion peaks reflects the existence of both mobile water and hydration water at the GMO−water interface (hydrogen exchange between the GMO hydroxyls and water molecules). Above 35 °C, the sample became fluid yet hexagonal symmetry was maintained. The fluidity of the H_{II} phase is explained by a significant reduction in the domain size and also perhaps cylinder length. This phenomenon was characterized by higher mobility of the GMO, lower mobility of the water, and a significant dehydration process.

Introduction

The phase behavior of mixtures of glycerol monooleate (GMO) and water is of great interest due to their widespread use in food and pharmaceutical products.[1−5] Depending on concentration and temperature, GMO and water can form a wide variety of mesophases: reversed micellar; lamellar; two reversed bicontinuous cubic phases, Q^{230} and Q^{224}, that form at room temperature; and a reverse hexagonal phase, H_{II}, that is obtained at relatively high temperatures (∼85 °C).[6−10] Subzero incubation produces the L_c ordered lamellar phase.[10] The high viscosity of the liquid crystalline phases limits their application and therefore raises the need for low-viscosity dispersions of liquid crystal phases in aqueous phase (e.g., cubosome, hexosome, and liposome dispersions).[11−13] However, while dilution with water lowers the viscosity, this process also dramatically decreases the solubilization capacity as well as the stability.[11−13] Lamellar and discrete cubic mesophases have been shown to exhibit lower viscosities compared to hexagonal and bicontinuous cubic phases. These more fluid materials have found application in several biophysical studies (lipolytic process and protein entrapment)[14−18] as well as for the production of bioelectrodes and biosensor constructs.[19−21] However, there is as yet no validated process for producing bulk H_{II} phases with low viscosity which fully utilizes the properties of the hexagonal phase. Therefore in the current work we aimed to obtain a lower viscosity reverse hexagonal phase and to explore its physical properties.

The typical idealized scheme of a reverse hexagonal phase containing amphiphilic molecules (surfactants) is that of infinitely long, relatively straight, circular cylinders arranged in a two-dimensional array. The amphiphilic molecules are perpendicular to the cylindrical interface with chains pointing outward and hydrophilic heads pointing inward toward a channel where water molecules can diffuse. The bulk, macroscopic hexagonal mesophase is polycrystalline with randomly oriented microdomains. Unlike the binary mixture of GMO with water, GMO/water with added tricaprylin (TAG) displays a reverse hexagonal phase at room temperature over a broad range of compositions.[22] Along the dilution line of 90/10 GMO/tricaprylin, this region can be divided in two, according to water content.[23] At water content below 20 wt % the hexagonal phase is less ordered, while, at higher concentrations up to 30 wt % water, the hexagonal phase is more ordered. As determined by small-angle X-ray scattering (SAXS), the higher degree of order in the more dilute liquid crystal is expressed by larger lattice constants and domain sizes.[23] Additionally, the less ordered H_{II} phase demonstrated lower viscosity with zero shear rate viscosity of the less ordered which was 4 times lower than the more ordered one (unpublished results).

In the present work, we examine the hexagonal phases of GMO/tricaprylin/12.5 wt % water at temperatures both above and below ambient. We follow the water-poor H_{II} phases, including samples with high and low viscosities, at relatively low and high temperatures (zero shear rate viscosities of 10^4 and 10^3 Pa·s, respectively; unpublished results). The techniques used are SAXS, which provides symmetry and unit cell size; self-diffusion- and ^{2}H NMR spectroscopy; and FT-IR spectroscopy. These spectroscopies have been used to study lyotropic liquid crystalline systems at the molecular level.[24−32] NMR self-diffusion measurements have mainly focused on cubic and

* To whom correspondence should be addressed. Telephone: 972-2-658-6574/5. Fax: 972-2-652-0262. E-mail: garti@vms.huji.ac.il.

[†] Casali Institute of Applied Chemistry, The Institute of Chemistry, The Hebrew University of Jerusalem.

[‡] The Weizmannn Institute of Science.

[§] Wolfson Centre for Applied Structural Biology, The Hebrew University of Jerusalem.

10.1021/jp076662t CCC: $37.00
Published on Web 11/08/2007

lamellar phases[24−31] and only recently on the hexagonal phase.[33] By concentrating on water diffusion[27,31] or deuterium quadrupole splitting,[34−38] these NMR studies indirectly characterized the microstructure. ^{2}H NMR identified anisotropic water populations, which implied either lamellar or hexagonal phases.[34−38] FTIR was used to follow phase transitions of the lyotropic liquid crystalline phases, primarily with binary systems.[39−42]

The aim of this work is to characterize the microstructure of the relatively low viscosity, less-ordered H_{II} structure as a function of temperature and to understand the factors that govern the formation of this phase. By doing so, it should be possible to expand this area in the ternary phase diagram and to improve the properties of the mixtures in a controlled manner with a view to eventual applications. Lower viscosity fluid hexagonal phases should have a broad range of uses, e.g., in injectable medications and for improved qualities of spreading and absorption in pastes.

Experimental Methods

Materials. Monoolein, GMO, distilled glycerol monooleate that consists of 97.1 wt % monoglyceride and 2.5 wt % diglyceride (acid value 1.2, iodine value 68.0, melting point 37.5 °C, and free glycerol 0.4%) was purchased from Riken (Tokyo, Japan). It should be noted that when other manufacturers or batches of GMO were used, similar results were obtained. Tricaprylin (triacylglycerols, TAG; assay 97−98%) was obtained from Sigma Chemical Co. (St. Louis, MO). D_2O (D, 99.9%) was purchased from Cambridge Isotope Laboratories, Inc. (Cambridge, MA). Water was double distilled. All ingredients were used without further purification.

Sample Preparation. The GMO/tricaprylin/water hexagonal liquid crystals were prepared by mixing weighed quantities of GMO, tricaprylin (90/10 weight ratio), and water while heating to ∼70 °C for ca. 15 min. This was done in sealed tubes under nitrogen atmosphere (to avoid oxidation of the GMO). The samples were stirred and cooled to 25 °C and were allowed to equilibrate for 24 h before examination.

Light Microscopy. The samples were inserted between two glass microscope slides and observed with a Nikon light microscope equipped with cross-polarizers and attached to a video camera and monitor. The samples were analyzed between room temperature and 50 °C.

Small-Angle X-ray Scattering. Scattering experiments were performed using Ni-filtered Cu Kα radiation (0.154) from an Elliott rotating anode X-ray generator that operated at a power rating of 1.2 kW. X-radiation was further monochromated and collimated by a single Franks mirror and a series of slits and height limiters and measured by a linear position-sensitive detector. The samples were held in 1.5 mm quartz X-ray capillaries inserted into a copper block sample holder. The temperature was maintained at $T \pm 0.5$ °C with a recirculating water bath. The camera constants were calibrated using anhydrous cholesterol. Prior to the diffraction measurements, the samples were incubated at subzero temperature for at least 2 h to facilitate full development of the L_c phase.

The scattering patterns were desmeared using the Lake procedure implemented in home-written software.[43] To estimate a lower bound for the sizes of ordered domains (L_H), the full width at half-height of the (10) diffraction peak was measured and this value was inserted into the Scherrer formula.[44]

Wide-Angle X-ray Scattering. Wide-angle X-ray scattering (WAXS) patterns from samples held in 1.5 mm quartz capillaries were obtained on Fuji imaging plates, using a Searle camera equipped with Franks optics, affixed to an Elliott GX6 rotating anode generator operating at 1.2 kW and producing copper radiation ($\lambda = 1.54$ Å). The capillaries were dusted with calcite as a distance calibrating material and inserted into a copper block, the temperature of which was controlled using a Peltier thermoelectric element (Melcor). Exposure times were on the order of 8 h. The imaging plates were scanned with a He−Ne laser (Spectra Physics-Lexel) in conjunction with a homemade reader based on an Optronics densitometer with computer interface. Prior to the diffraction measurements, the samples were incubated at subzero temperature overnight to facilitate full development of the L_c phase.

Differential Scanning Calorimetry. A Mettler Toledo DSC822 measuring model system was used. The differential scanning calorimetry (DSC) measurements were carried out as follows: 5−15 mg hexagonal liquid crystalline samples were weighed, using a Mettler M3 microbalance, in standard 40 μL aluminum pans and immediately sealed by a press. The samples were rapidly cooled in liquid nitrogen from +30 to −20 °C, at a rate of 4 °C min^{-1}. The samples remained at this temperature for 120 min and then were heated at 1 °C min^{-1} to 40 °C. An empty pan was used as a reference. The instrument determined the fusion temperatures of the components and the total heat transferred in any of the observed thermal processes. The enthalpy change associated with each thermal transition was obtained by integrating the area of the relevant DSC peak. DSC temperatures reported here were reproducible to ±0.2 °C.

Pulsed-Gradient Spin−Echo NMR. The field gradient stimulated pulse−spin−echo program (PGSE-NMR) was used to measure diffusion. The measurements were performed on samples between −10 and +40 °C on a Bruker DRX-400 spectrometer, with a BGU II gradient amplifier unit and a 5 mm BBI probe equipped with a *z*-gradient coil, providing a *z*-gradient strength (g) of up to 55 G cm^{-1}. Experiments were carried out by varying g and keeping all other timing parameters constant. The measurements were repeated at least 3 times. According to the parameters of the experiments (the time between the leading edges of the gradient pulses, Δ, was 300 ms), the possible molecular displacement during the experiment, $\langle r^2 \rangle = 2\Delta D$, is on the order of 1 μm or more. The substructures are smaller than this such that the measured diffusion coefficient represents the aggregate diffusion.[45,46]

^{2}H NMR. Samples for NMR experiments were prepared using 4% D_2O as part of the water component. The NMR experiments were performed on a Bruker DRX 600 MHz spectrometer operating at a proton frequency of 600 MHz and deuterium frequency of 61.42 MHz, using a 5 mm broadband probe. The proton and deuterium spectra were acquired with 8K and 2K points, with spectral widths of 13 and 200 ppm, respectively. The temperature range between −10 and +60 °C was precise to within 0.2 °C, and samples were allowed to equilibrate for 10 min at each temperature. The spectra were acquired using 16 transients, exponential apodization with line broadening of 20 Hz, and zero filling of 8K and 4K, respectively.

The magnitude of the quadrupolar splitting is shown to follow[47]

$$\Delta = \left| \sum P_i(\upsilon_{Q_i}) S_i \right| \tag{1}$$

where S_i is the order parameter of bound water describing the orientation of the fraction of ^{2}H present at site i (P_i). υ_Q is the quadrupolar coupling constant (220 kHz).[47,48] The magnitude of the quadrupolar splitting has been shown to be proportional to the order parameter.[47,48]

Attenuated Total Reflectance Fourier Transform Infrared. A ReactIR 4000 model (Millersville) manufactured by Mettler-

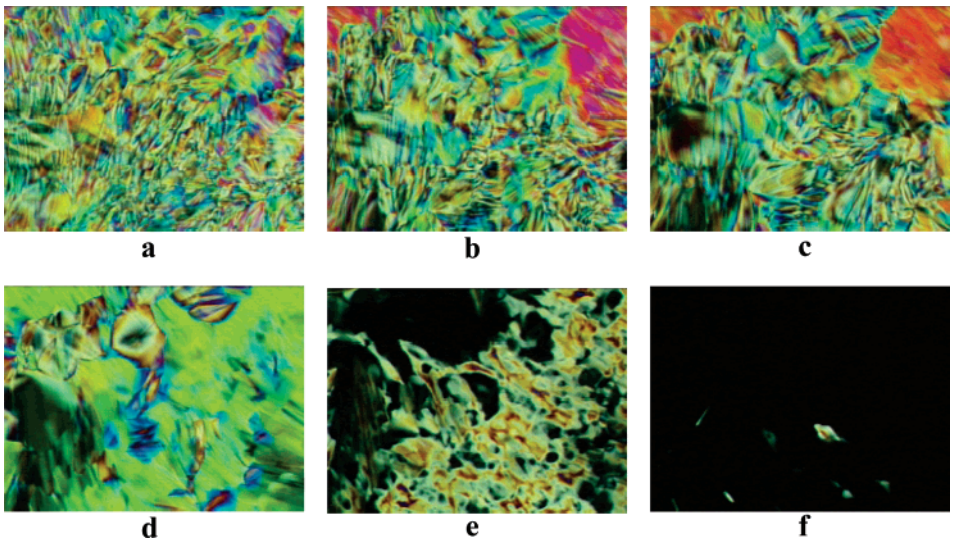

Figure 1. Polarized optical microscope images of the H_{II} liquid crystal phases at (a) 24.1, (b) 31.5, (c) 35.0, (d) 40.0, (e) 45.0, and (f) 48.5 °C.

Toledo equipped with a diamond probe (DiComp) was used to record the attenuated total reflectance Fourier transform infrared (ATR FTIR) spectra (pure components and GMO/TAG/water mixture). The spectra were recorded with 128 scans. The probe was purged with dry air. The procedures were conducted in the 0.6 L glass reactor of the Mettler-Toledo LABMAX system (Schwerzenbach, Switzerland) which includes a glass reactor, propeller stirrer, thermostat unit, and controller unit. The thermostat unit controls the reactor and jacket temperature on the basis of feedback from the temperature sensors in the reactor and in the jacket. Temperature can be controlled either by specifying an end point temperature or by keeping a predetermined temperature difference between the reactor and the jacket. The samples were first heated to +60 °C for 30 min and then cooled to −10 °C (0.25−1 °C min^{-1} for relatively low and high temperatures, respectively) for 2 h. In the measurements of FTIR spectra as a function of temperature, the mixture was heated stepwise with temperature intervals of 5 °C. After the sample was kept at the desired temperature for 0.5−1 h, the spectra were recorded. The absorbance intensities reported here were reproducible to ±0.005.

Results and Discussion

Temperature Dependence of the Bulk Properties of the Water-Poor Reverse Hexagonal Phase. The H_{II} liquid crystals formed at room temperature by GMO/tricaprylin/water mixtures with water content below 20 wt % are characterized by smaller lattice parameters (52.3 ± 0.5 Å) and effective crystallite sizes (772 ± 50 Å) relative to the more ordered, water-diluted (25 wt %) mixtures (55.4 and 1014, respectively).[22−23] Measurement of the room-temperature viscoelastic properties of these less-ordered H_{II} structures revealed that a decrease in water content is accompanied by a decrease in viscosity (zero shear rate viscosity of the less ordered was 4 times lower than the more ordered one, unpublished results). Incrementally raising the water concentration dramatically increased the viscosity, thereby limiting our ability to examine this region. Instead, we varied the temperature in order to effectively extend the range of the low-viscosity H_{II} phase.

Polarized Light Microscopy. A sample composed of GMO/TAG (90/10 surfactant to oil weight ratio), with 12.5 wt % water was studied by polarized light microscopy in the temperature range between 24.1 and 48.5 °C. Parts a−f of Figure 1 show the polarized light microscope images at 24.1, 31.5, 35.0, 40.0, 45.0, and 48.5 °C. Up to 35.0 °C, the material displayed birefringent and colorful textures typical of hexagonal symmetry. At 35.0 °C, the sample is fluid (we can detect the sample flow during the measurement) and black regions appeared in addition to the hexagonal texture (Figure 1c). Above this temperature, the disappearance of the hexagonal phase continues up to 48.5 °C (Figure 1f), where most of the hexagonal phase texture has been replaced by black regions. The absence of texture is consistent with the appearance of the L_2 phase.[10]

DSC. A typical DSC thermogram obtained during heating a GMO/TAG/12.5 wt % water mixture is shown in Figure 2. The thermotropic behavior of this mixture during the heating scan from −20 to +40 °C reveals two rather broad endothermic events with maxima at −1.0 ± 0.2 (peak A) and 6.1 ± 0.2 °C (peak B). There is an additional high-temperature shoulder on peak B and a broad plateau which extends from approximately 12 to 26 °C. Identification of the two peaks was discussed previously (at higher water content).[23] It was found that peak A is related to the fusion of water (with enthalpy of 24 J g^{-1}) and peak B is related to the fusion of the hydrophobic moieties of the GMO affected by TAG (36 J g^{-1}). The subzero temperature of peak A indicates the presence of bound water at this water concentration (12.5 wt %). The position of peak B is determined by the relative miscibility of one component in the other (hydrophobic interactions or solvation of the GMO tails by the TAG molecules) during the heating process. Increasing the GMO concentration leads to higher melting temperatures and vice versa.[23] We conclude that below −1.0 ± 0.2 °C both the water and the surfactant hydrophobic moieties are crystalline. Above 12 °C (end set of peak B) most of the material has melted, although this process may not be complete until ∼26 °C.

WAXS and SAXS. X-ray scattering was used to identify or confirm the structure of the different phases in relation to the boundaries defined by the endothermic peaks of the DSC thermogram. Measurements were made during heating from 3 to 45 °C, following overnight incubation at subzero temperature. Parts a−g of Figure 3 show the X-ray scattering patterns of the GMO/TAG/12.5 wt % water mixture at 3 °C (2D WAXS) and at 7, 16, 25, 36, 40, and 50 °C (1D SAXS). At 3 °C (Figure 3a), i.e., below the maximum of peak B, a 2D WAXS image revealed four low-angle partially oriented reflections which

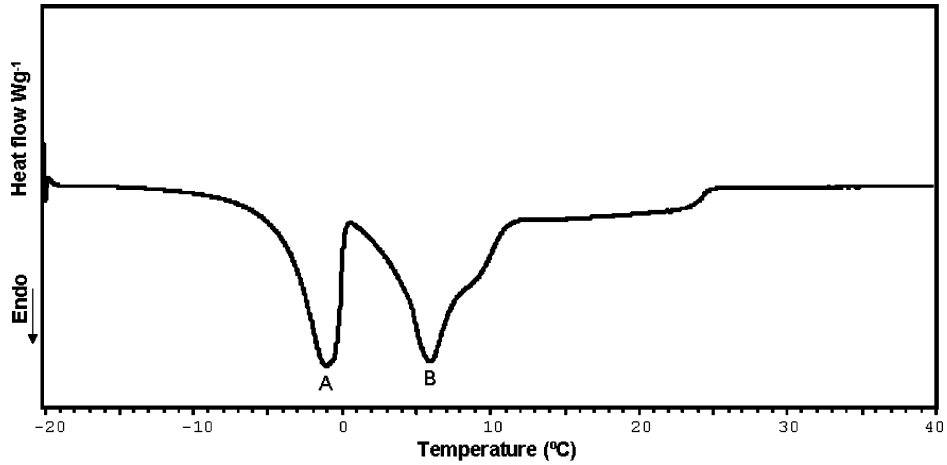

Figure 2. DSC thermogram of GMO/tricaprylin/water mixture with two endothermic events at -1.0 ± 0.2 (peak A) and 6.1 ± 0.2 °C (peak B).

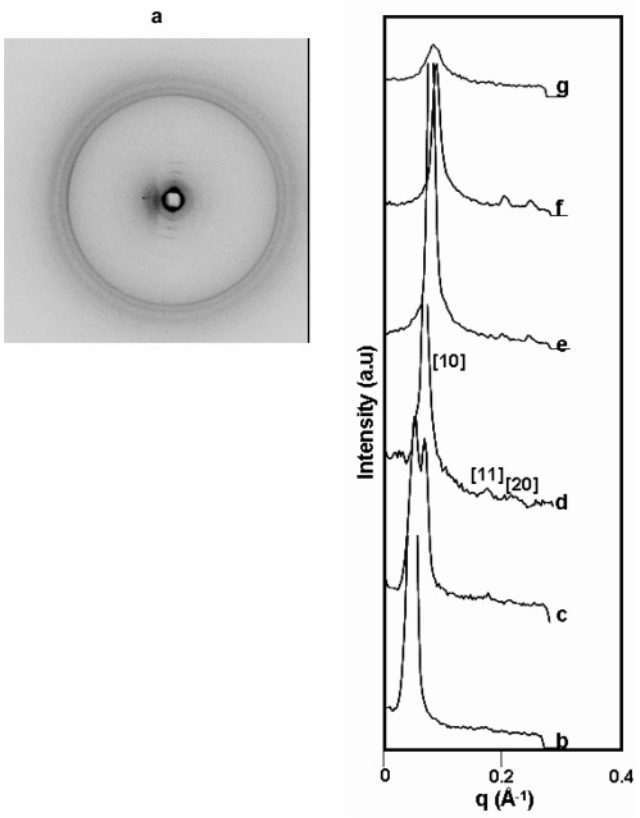

Figure 3. X-ray diffraction patterns of the 90/10 GMO/tricaprylin mixture with 12.5 wt % water after overnight incubation at −20 °C and measured at (a) 3 °C (2D WAXS) and (b) 7, (c) 16, (d) 25, (e) 36, (f) 40, and (g) 50 °C (1D SAXS).

could be indexed as the first four orders of a lamellar phase with interlamellar spacing of 49 Å. In addition there are a number of wide-angle peaks at 4.59, 4.32, and 4.06 Å. The latter are characteristic of a crystalline low-temperature phase, L_c.[10] Such a phase has been previously identified for GMO/water mixtures following extended low-temperature incubation.[10] At 7 °C (Figure 3b), the SAXS profile shows a single Bragg peak at 49 Å which can be associated with the lamellar phase observed in the WAXS image. At 16 °C, the SAXS profile gives evidence of a biphasic region. The 49 Å peak of the L_c phase is present as is the (10) reflection of the nascent hexagonal phase. At temperatures above 16 °C, three peaks are observed, which can be indexed as the (10), (11), and (20) reflections of a 2D hexagonal liquid crystalline phase. Such a structure is visualized as consisting of cylindrical surfactant micelles arranged on a 2D hexagonal lattice.[49] From the three peak positions and the (10) peak line breadth, we calculated the corresponding mean lattice parameter (a) and the effective crystallite size (L_H) of the hexagonal structures. The results are summarized in Table 1.

TABLE 1: Lattice Parameters and the Effective Crystallite Sizes (a and L_H, Respectively) of the Hexagonal Structures in GMO/TAG/water Mixture (12.5 wt % Water Concentration) as a Function of Temperature

temp ± 0.5 (°C)	$a \pm 0.5$ (Å)	$L_H \pm 50$ (Å)
10.0	50.1	not detectable
16.0	48.4	625
20.5	46.6	616
25.3	46.5	634
28.1	46.4	557
35.7	45.4	372
39.5	44.3	385
45.0	not detectable	315
50.0	not detectable	220

Upon increasing the temperature, the lattice parameter decreased. Between 20 and 28 °C the decrease was small, while at higher temperatures (36−40 °C) it was more pronounced (Table 1). The decrease in the lattice parameter with increasing temperature can be explained either by dehydration of the surfactant polar headgroups or by an increase in the hydrocarbon chain mobility.[10,23,24] The decrease in L_H upon increasing temperature (634−385 Å) was most pronounced between 26 and 40 °C. Previously we reported that addition of a hydrophilic polymer, which competed for water with the GMO polar headgroups, led to a dehydration process.[23] This led to a reduction in L_H and in the lattice parameter values. At this point, we may assume that the elevated temperature which increased the mobility of both water and GMO chains results in increasing the critical packing parameter (CPP) value and dehydrating part of the hydration water.[10,23,24] Hence, the hexagonal phase, which is strongly dependent on hydrogen bonding, gradually shrank to complete disruption while the curvature and CPP values increased.

The three analytical methods (polarized light microscopy, SAXS, and DSC) provide evidence that at elevated temperatures (35−40 °C) the liquid crystal H_{II} phase is less ordered than at room temperature, with a 40% smaller effective crystallite size and partially dehydrated head groups. It is possible that these changes are a prelude to the $H_{II}-L_2$ transformation which takes place above 45 °C (Figure 3g, Table 1).

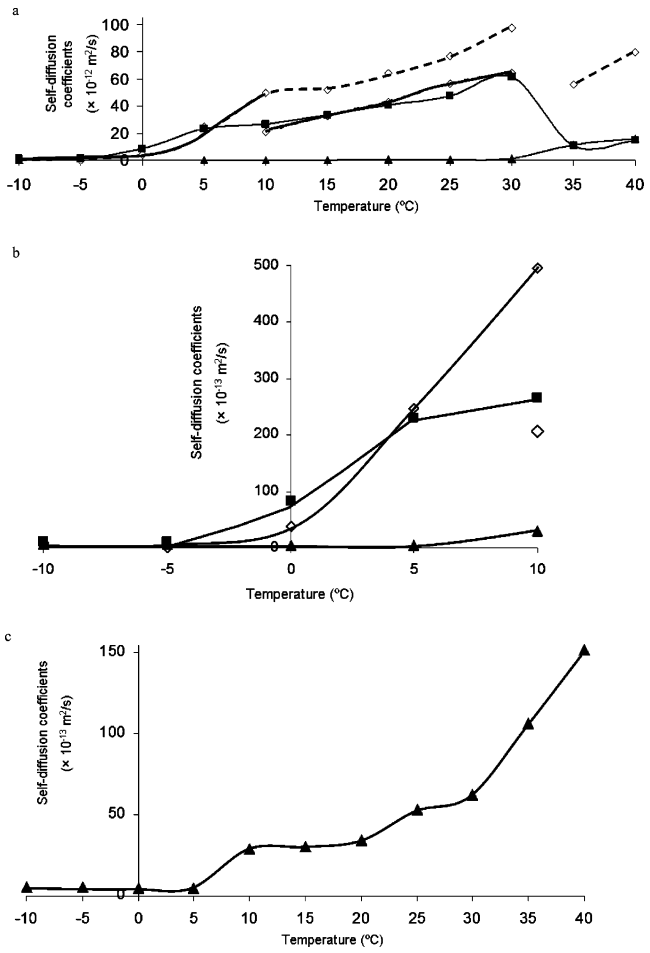

Figure 4. Self-diffusion coefficients of (a) water (symbol ◇, dashed line for free water and solid line for hydration water), TAG (■), and GMO (▲), from −10 to +40 °C; (b) water (symbol ◇, solid line for hydration water), TAG (■), and GMO (▲), from −10 to +10 °C; and (c) GMO (▲) from −10 to +40 °C, measured by means of the ^{1}H NMR PFGSE technique for the GMO/TAG/water (12.5 wt % water) mixture.

Temperature Dependence of the Microstructure of the Water-Poor Reverse Hexagonal Phase. We used PGSE NMR, ^{2}H NMR, and FTIR spectroscopy to characterize the microstructure of the low water content H_{II} structure as a function of temperature.

PGSE-NMR. The self-diffusion coefficients of water (D_W), TAG (D_{TAG}), and GMO (D_{GMO}) measured using the ^{1}H NMR PGSE technique, between −10 and +40 °C for the GMO/TAG/12.5%water mixture are shown in Figure 4a−c. The diffusion coefficients characterize the mobility of the three components of the mesophase in four temperature regions: −10 to 0, 0 to +10, +10 to +30, and +30 to +40 °C.

Temperature Range of −10 to 0 °C. In this temperature range, D_W and D_{GMO} are of the order of magnitude of 10^{-13} m^2 s^{-1} in contrast to D_{TAG}, which is of the order of magnitude of 10^{-12} m^2/s (Figure 4a,b). Between −5 and 0 °C the water diffusion coefficient increased by a factor of 10, presumably due to melting of the bound water. During this process the water molecules would be expected to hydrogen bond to GMO, thereby restricting their motion. We suspect that at this temperature TAG is incorporated at the end of the tails of the GMO molecules because its diffusion coefficient is significantly larger than that of GMO.

Temperature Range of 0 to +10 °C. Further heating of the mixture led to an increase in the diffusion coefficients of all the components (Figure 4a,b). Up to 5 °C, D_{GMO} is much smaller than both D_W and D_{TAG}. A further increase in the diffusivity of the water was detected (from 10^{-12} to 10^{-11} m^2 s^{-1}), suggesting the presence of free water as well. The DSC measurements detected weakly bound water that melts at ca. −1 °C. The diffusion coefficients of the GMO are the lowest of the three components; however, an increase from 10^{-13} to 10^{-12} m^2 s^{-1} can be seen during heating from 5 to 10 °C. The increase in the GMO and in the TAG molecules' mobility can be associated with the transition of the hydrocarbon chains from a rigid conformation to one which is liquid-like. These results are in agreement with the DSC peak at 6.1 ± 0.2°C attributed to the melting of hydrophobic moieties (peak B in Figure 2). The X-ray measurement at 3 °C supports the presence of the L_c phase prior to the hydrophobic transition (peak B).

Temperature Range of +10 to +30 °C. Increasing the temperature to 30 °C increased the mobility of all three components. Beginning at 10 °C the measurements detect two populations of water molecules with quite different diffusion coefficients (Figure 4a). For example, at 10 °C the water self-diffusion coefficients were 49.6 × 10^{-12} and 20.6 × 10^{-12} m^2 s^{-1}, and at 30 °C these increased to 97.7 × 10^{-12} and 64.6 × 10^{-12} m^2 s^{-1}. Since water is insoluble in TAG, practically all the water must be found in the interior of the surfactant aggregates. As shown by the X-ray data (Figure 2), cylinders become the dominant aggregate form above 16 °C. One population of water molecules is bound to the surfactant headgroups, with a smaller diffusion coefficient, while a second population is more free to diffuse along the axis of the cylinder. Coppola et al. examined the pentaethylene glycol dodecyl ether/water/decane/sodium dodecyl sulfate mixture at 45−50 °C.[33] He made the assumption that the water molecules exist as both free and bound water, in rapid exchange, and that the bound water has the same mobility as the surfactant.[33] However, in our measurements, in the range of temperature between 10 and 30 °C, we can identify two separate NMR signals for water due to hydrogen exchange between the GMO hydroxyls and the water molecules; hence, such an assumption is unnecessary. This is similar to what Liu et al.[37] report for the bis(2-ethylhexyl) sodium sulfosuccinate/lecithin/isooctane system at 25 °C

The increase in the mobility of the TAG molecules with increasing temperature is associated with the complete transition of the hydrocarbon chains to a liquid-like conformation. The GMO self-diffusion coefficients are an order of magnitude lower than the values found for water or TAG. Additionally, the GMO self-diffusion coefficients depend less strictly on the temperature, being almost constant in this temperature region.

Temperature Range of +30 to +40 °C. Further heating of the mixture from 30 to 35 °C, at which temperature the sample flows like a liquid while maintaining hexagonal symmetry, results in modification of all the diffusion coefficients (Figure 4a,c). The diffusion coefficient of TAG decreased from 61.4 × 10^{-12} to 10.5 × 10^{-12} m^2 s^{-1}, matching that of GMO. In this temperature range TAG is fully miscible with GMO. The two diffusion peaks of the water merge into a single peak with a corresponding diffusion coefficient of 56.0 × 10^{-12} m^2 s^{-1}. At these temperatures we can assume that the water molecules exist as free and bound water in rapid exchange; hence, the water diffusion coefficient would be an average of the bound and free water. Furthermore, dehydration with increasing temperature is expected and has been studied in several systems.[10,24,50]

The decreasing water self-diffusion coefficient can be explained in terms of reduced water mobility and may suggest shorter channel lengths, as a prelude to the H_{II}−L_2 transforma-

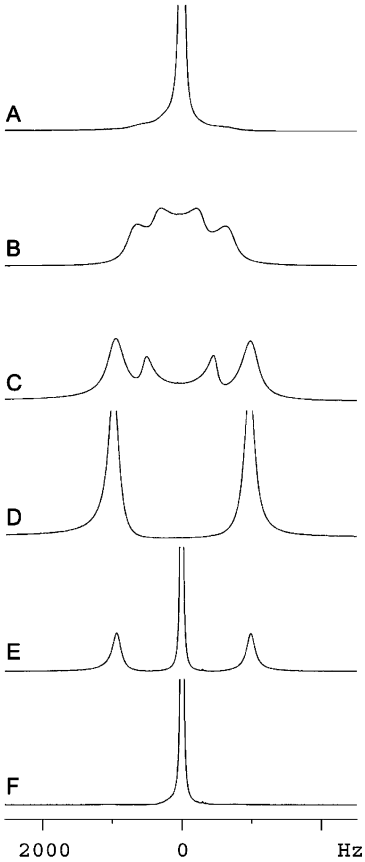

Figure 5. ^{2}H NMR quadrupolar splitting at (A) −5, (B) 10, (C) 25, (D) 35, (E) 40, and (F) 45 °C.

tion which takes place at ∼45 °C. This behavior is consistent with data reported by Coppola at al.[33] who observed a structural change for the pentaethylene glycol dodecyl ether/water/decane/sodium dodecyl sulfate mixture at the $L_3 \rightarrow H_2$ transition (∼45 °C).[33]

^{2}H NMR. We measured the ^{2}H NMR quadrupolar splitting over the temperature range from −10 to +40 °C for the GMO/TAG/D_2O−H_2O (12.5 wt % water, of which 4% was deuterium oxide) mixture. Prior to measurement, the sample was heated to 60 °C (the isotropic phase), followed by cooling to −20 °C during 10 h. The magnitude of the quadrupolar splitting has been shown to be proportional to the order parameter (see the Experimental Methods).[48] The quadrupolar splitting at −5, 10, 25, 35, 40, and 45 °C is shown in Figure 5A−F.

The superposition of weak peaks with quadrupolar splitting of 1100 Hz and an isotropic peak for the samples in the temperature range of −10−5 °C is shown in Figure 5A. The former is consistent with the existence of an anisotropic phase (L_c as detected by X-ray). The strong isotropic peak may imply the presence of ice as was noted by Caffrey.[10] Increasing the temperature to 10 °C led to the disappearance of the isotropic peak which may suggest that the water incorporation in the surfactant aggregates was completed (see Figure 5B). At 10 °C two quadrupolar splittings are observed at 960 and 1930 Hz. SAXS data confirm the coexistence of a lamellar and hexagonal phase at this temperature. Raising the temperature to 25 °C led to the reduction of the relative intensity of the peaks with the smaller splitting while simultaneously increasing the larger splitting (Figure 5B,C, respectively). At 30−35 °C a single quadrupolar splitting can be detected at ∼2000 Hz, which implies a single anisotropic environment for the deuterium (Figure 5D). We can conclude that the cylinders of the H_{II} phase are aligned with respect to the magnetic field of the spectrometer.[34−38] It is possible that the increased fluidity of the H_{II} phase at this temperature facilitates alignment. Upon further heating of the mixture to 40 °C an isotropic peak appeared in addition to the split pair (Figure 5E). Above 40 °C only a single sharp isotropic peak can be seen in Figure 5F. This result is consistent with the formation of the L_2 phase which was revealed by SAXS.

FTIR. The molecular structure of GMO and the FTIR spectrum for the GMO/TAG/12.5 wt % water mixture at 25 °C are shown in Figure 6. We focused on seven major bands indicated in the figure to analyze the conformation of the surfactant molecule and its interaction with the water in the different mesophases as a function of temperature (−10 to +40 °C).

We analyzed the structure in terms of three regions: the water-rich core, the water−surfactant interface, and the lipophilic acyl chain region. The absorption bands at 3200−3400 cm^{-1}, which are attributed to the O−H stretching modes (ν_{OH}), are used to characterize the interactions of the O−H groups (at the β and γ positions on the GMO headgroups) of the surfactant and water molecules. The stronger the hydrogen-bonding between the surfactant and the water, the lower the stretching frequency of O−H group (ν_{OH}). At the interface, four vibrational modes could be recorded reflecting the interfacial arrangement of the lipid headgroups. For GMO, these include the stretching of the bonds CO−O (ester at the α position, ∼1180 cm^{-1}), C−OH (β, ∼1121 cm^{-1}), C−OH (γ, ∼1046 cm^{-1}), and C═O (carbonyl at the α position, 1720−1740 cm^{-1}).[42,51,52] The carbonyl band consists of two components, one originating from "free" (freely rotating) carbonyl (1740 cm^{-1}) and the second, from intramolecular hydrogen-bonded carbonyl groups (1730 cm^{-1}).[42,51] Information about the conformational order of the acyl chains is obtained from the stretching modes of the CH_2 segments (ν_{CH_2}). The stretching modes of the GMO methylene groups are observed at ∼2853 cm^{-1} (symmetric stretching) and at ∼2918 cm^{-1} (antisymmetric stretching).[42,51]

Water-Rich Core. The temperature dependence of the infrared spectra of the GMO/TAG/water mixture in the range of 3000−3700 cm^{-1} can be seen in Figure 7a. Between −10 and −5 °C two poorly resolved maxima of the O−H (β and γ positions of GMO) stretching absorption bands are detected at 3238 and 3296 cm^{-1}, respectively. The lower ν_{OH} is attributed to the less hydrated O−H group (β position); however, the low frequencies of both groups can imply strong hydrogen bonds at these temperatures. When the temperature is raised beyond −5 °C the ν_{OH}-values increased by 60 and 70 cm^{-1}, for the β and γ positions, respectively. Between −5 and +15 °C the absorption intensity of the O−H (γ position) group exceeds that of the O−H absorption at the β position. This indicates that a fraction of the hydrogen bonds between O−H groups (γ position) and water molecules are broken at this temperature (−5 to 0 °C), similar to the bound water melting which was detected by DSC.[39] At 15 °C, an additional small decrease (∼8−16 cm^{-1}) in the ν_{OH} frequencies can be detected. This reduction in frequency may be explained through the restriction of the headgroup surface area due to increasing curvature and H_{II} formation.[51] However, increasing the temperature led to a further increase in the O−H stretching frequencies, as expected. Above 30 °C, due to the expected dehydration of the headgroups one should anticipate a further increase in the stretching vibration.[39] However, the frequencies slightly decreased (∼6 cm^{-1}) possibly suggesting the existence of more restricted surface.[42]

Water−Surfactant Interface. The positions of the C−OH (β, ∼1121 cm^{-1}) and C−OH (γ, ∼1046 cm^{-1}) stretching frequen-

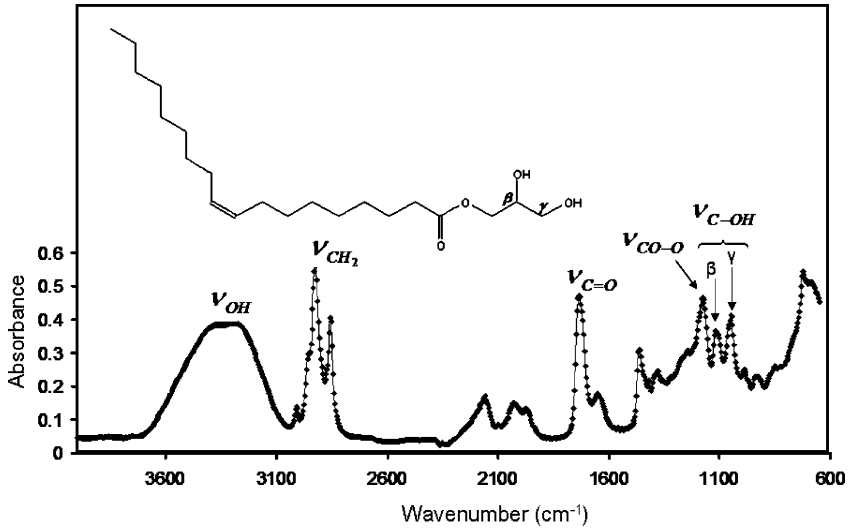

Figure 6. IR spectrum obtained for GMO/TAG/water mixture with 12.5 wt % water at 25 °C. The symbols marked on several absorption bands are explained in the text.

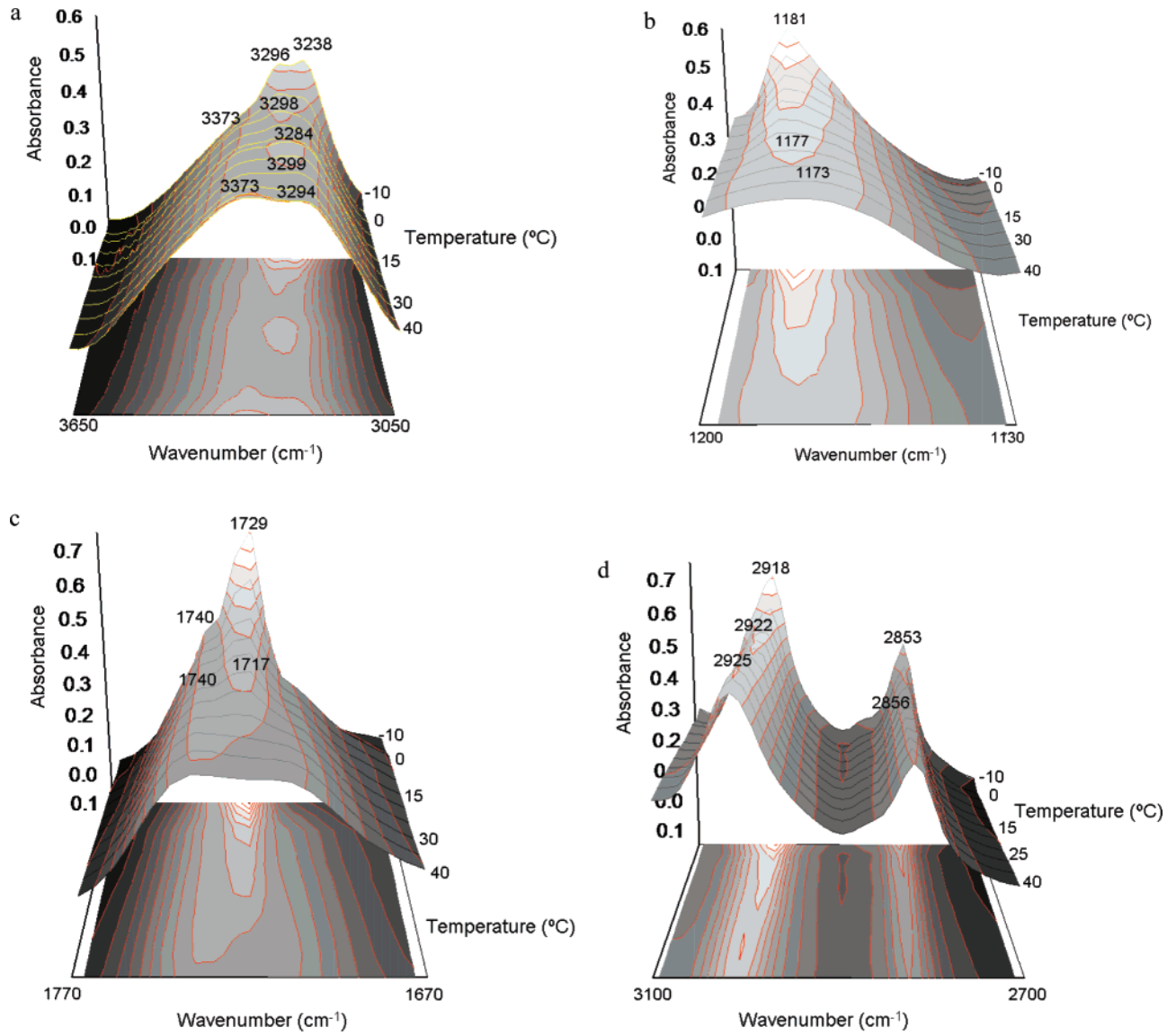

Figure 7. IR spectra obtained for GMO/TAG/water mixture at various temperatures between −10 and +40 °C in the frequency ranges: (a) 3000−3600, (b) 1130−1200, (c) 1670−1770, and (d) 2700−3100 cm^{-1}. Temperatures (°C) are indicated in the figure.

cies were only weakly affected by the temperature-induced changes in the structure of the GMO/TAG/water mixture (data not shown). On the other hand, the $C_\alpha O-O$ stretching mode (~1180 cm^{-1}) was apparently sensitive to the lamellar−

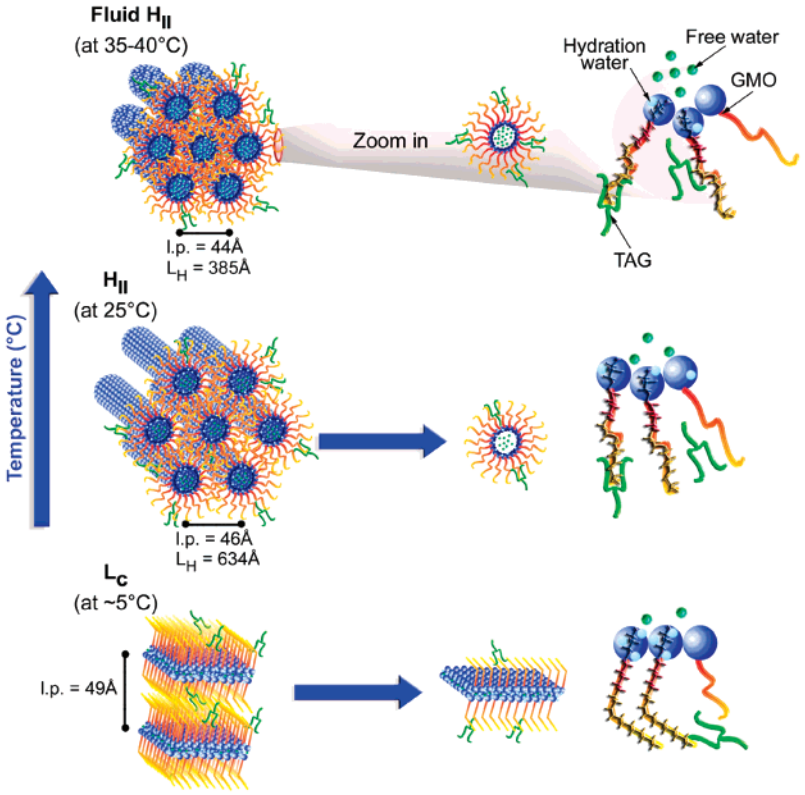

Figure 8. Schematic presentation illustrating the structural and physicochemical properties of the mesophases as a function of temperature. l.p. and L_H correspond to the mean lattice parameter and the effective crystalline size of the mesophases.

hexagonal transition and to the reduction in the domain size of the H_{II} liquid crystals (Figure 7b). Up to 15 °C, the maximum ester group stretching absorption was detected at 1181 cm^{-1}, while the peak height decreased and the line width increased with increasing temperature. Above 15 °C the frequency decreased to 1177 cm^{-1}, and a further increase in temperature to 35 °C resulted in an additional decrease to 1173 cm^{-1}. It has been proposed[51,53] that a low-frequency shift of the CO−O band may be interpreted as a slight deviation from the dihedral angle of 180° in the $C_\gamma-C_\beta-C_\alpha O-O-C$ segment, induced by torsional motions or by a small population of gauche conformers near the CO−O bond.[51,53] It should be pointed out that, for pure GMO and TAG, the CO−O band is found at 1180 and 1156 cm^{-1}, respectively (at room temperature). Following this interpretation and according to the pure GMO and TAG data, we can conclude that TAG and the temperature have a similar effect on the dihedral angle in GMO. This is consistent with the fact that they both increase the curvature and lead to a more restricted interface with the formation of H_{II} and low-viscosity H_{II} compared to the lamellar crystalline phase and even compared to the L_α phase at room temperature.[51]

The changes in the carbonyl bands as a function of temperature are shown in Figure 7c. Up to 15 °C, the major carbonyl band ($\nu_{C=O}$) was detected at 1729 cm^{-1} with an additional shoulder at 1740 cm^{-1}. Upon increasing the temperature from −10 to +15 °C, the intensity of the free carbonyl increased at the expense of the hydrogen-bonded carbonyl (lower $\nu_{C=O}$). Raising the temperature above 15 °C caused the lower frequency C═O band to transform into a shoulder, with an additional shift to 1717 cm^{-1}. Simultaneously, the intensity of the free carbonyl stretching band increased and remained at 1740 cm^{-1}. Hydrogen bonding is known to be responsible for the shift to lower frequency.[51] These results are in agreement with the $C_\alpha O-O$ stretching modification, implying that above 15 °C there is a significant modification in the hydration level. It is known that dehydration takes place once the H_{II} phase is formed and as the temperature increases, and in both cases the headgroup surface area decreases.[24,50] We can conclude that at this stage the water is partially bound to the carbonyl groups. However, further increasing the temperature gradually raised the stretching frequencies, and therefore the dehydration continues up to 35 °C. At 35 °C, the intensity of the less hydrated carbonyl vibrations slightly decreased, and the more hydrated carbonyl band shifted to higher frequencies (4 cm^{-1}), indicating an additional dehydration process. However, the total downward shift at the lowest temperature (4 cm^{-1}) suggests that although the GMO is dehydrated at elevated temperatures, the interface is more packed, probably due to a further increase in the curvature. As can be anticipated, this tendency is more pronounced in the transformation from the L_c to H_{II} phase than from H_{II} to liquefied H_{II}.

Hydrocarbon Chain Region. At −10 °C, the methylene stretching ν_{CH_2} of the hydrocarbon chains of GMO were observed (Figure 7d) at ~2853 cm^{-1} (symmetric stretching) and at ~2918 cm^{-1} (asymmetric stretching). Following the behavior of the asymmetric stretching mode with temperature reveals an upward shift (4 cm^{-1}) at 5 °C, while the symmetric stretching mode shifted to higher frequencies (3 cm^{-1}) only at 15 °C. It is known[39,42] that ν_{CH_2} is sensitive to the conformation of the hydrocarbon chain and it shifts upward with an increase in the fraction of gauche conformers. The latter results in increased chain disorder and looser acyl chain packing.[42] Thus, we can identify the chain melting in the range of 5−15 °C. Above 25 °C, the asymmetric stretching mode shifts 3 cm^{-1} to higher frequency, while the symmetric stretching frequencies remain constant. It should be mentioned that, in the absence of TAG, the symmetric and asymmetric stretching modes in the L_α phase of GMO/10 wt % water at 25 °C were found by Nilsson and co-workers[42] to be at 2853 and 2925 cm^{-1}, respectively. We can conclude that in the L_c phase (<5 °C) the tricaprylin is not

incorporated between the GMO tails as was suggested earlier from the SD-NMR results.

Conclusions

In the current study we used optical microscopy, WAXS, SAXS, and DSC to characterize the structural properties and interrelationships of the different components of a GMO/TAG/water liquid crystalline formulation. The NMR (self-diffusion and ^{2}H NMR) and FTIR measurements were used to evaluate conformational modifications at the molecular level. We were able to show that the GMO/TAG/12.5 wt % water mixture may undergo interrelated structural changes as a function of temperature that can lead to the formation of a fluid H_{II} phase that has very valuable physical characteristics and properties.

A cartoon of the different modifications of the ternary mixture as a function of temperature is shown in Figure 8. The details of the cartoon are drawn from the results of the experimental techniques described above. Following low-temperature incubation, the ternary mixture self-associates into the L_c phase which is stable between −10 and +5 °C (Figure 8 lower part). In the L_c structure the hydrocarbon chains are confined and tightly packed (WAXS), and hence their diffusion coefficient was the smallest (SD-NMR). The CH_2 asymmetric and symmetric stretching vibrations (FTIR) revealed an increase in the gauche conformer fractions at 5 and 15 °C, respectively, in parallel with the melting of the GMO hydrocarbon chains that was detected by DSC.

The lamellar crystal structure is gradually transformed with increasing temperature into a reverse hexagonal liquid crystalline phase (>10 °C, Figure 8 center). The hexagonal phase is formed due to increasing curvature of the surfactant interfacial region (higher CPP values). The presence of TAG molecules assists in the L_c-H_{II} transformation, hence TAG lowers the transformation temperatures (∼20 and ∼80 °C lower than for L_α and H_{II} phases in the GMO/water system, respectively). The hexagonal mesophase exhibits relatively rapid flow of water in the inner channels within the densely packed cylindrical shaped aggregates of GMO. The existence of a second slower diffusion constant also indicates the presence of hydration water at the GMO−water interface (hydrogen exchange between the GMO hydroxyls and water molecules). With increasing temperature, the surfactant headgroups are dehydrated and the hydrocarbon chain mobility is enhanced, both resulting in reduction of the lattice parameter. Above 35 °C additional structural changes occur. The sample is liquefied yet the hexagonal symmetry is maintained (Figure 8, upper part). The fluidity of the hexagonal phase was explained by the significant reduction in the domain size and cylinder length. This phenomenon is characterized by higher mobility of the GMO (SD-NMR and FT-IR) and lower mobility of the water (SD-NMR), and a significant dehydration process (FTIR). Characterizing the liquefied H_{II} structure at elevated temperatures (>35 °C) with respect to both the bulk and molecular scale properties will assist in the effort to expand this area in the room-temperature phase diagram in a controlled manner with a view to eventual applications, e.g., injectable medications and enhanced spreading and absorption qualities in pastes.

Acknowledgment. We would like to thank Dr. Uzi Eliav of Tel-Aviv University for helpful discussions on anisotropy in NMR.

References and Notes

(1) Larsson, K. *Lipids-Molecular Organization, Physical Functions and Technical Applications*; The Oily Press: Dundee, U.K. 1994.
(2) Krog, N. In *Food Emulsions*; Larsson, K., Friberg, S., Eds.; Dekker: New York, 1997; p 141.
(3) Clogston, J.; Rathman, J.; Tomasko, D.; Walker, H.; Caffrey, M. *Chem. Phys. Lipids* **2000**, *107*, 191−220.
(4) Mele, S.; Murgia, S.; Caboi, F.; Monduzzi, M. *Langmuir* **2004**, *20*, 5241−5246.
(5) Imura, T.; Hikosaka, Y.; Worakitkanchanakul, W.; Sakai, H.; Abe, M.; Konishi, M.; Minamikawa, H.; Kitamoto, D. *Langmuir* **2007**, *23*, 1659−663.
(6) Larsson, K. *J. Phys. Chem.* **1989**, *93*, 7304−7314.
(7) Larsson, K. K.; Fontell, K.; Krog, N. *Chem. Phys. Lipids* **1980**, *27*, 321−328.
(8) Qui, H.; Caffrey, M. *Biomaterials* **2000**, *21*, 223−234.
(9) Misquitta, Y.; Caffrey, M. *Biophys. J.* **2001**, *81*, 1047−1058.
(10) Caffrey, M. *Biochemistry* **1987**, *26*, 6349−6363.
(11) Rangelov, S.; Almgren, M. *J. Phys. Chem. B* **2005**, *109*, 3921−3929.
(12) Dong, Y. D.; Larson, I.; Hanley, T.; Boyd, B. J. *Langmuir* **2006**, *22*, 9512−9518.
(13) Almgren, M.; Borné, J.; Feitosa, E.; Khan, A.; Lindman, B. *Langmuir* **2007**, *23*, 2768−2777.
(14) Ericsson, B.; Larsson, K.; Fontell, K. *Biochim. Biophys. Acta* **1983**, *729*, 23−27.
(15) Razumas, V.; Larsson, K.; Miezis, Y.; Nylander, T. *J. Phys. Chem.* **1996**, *100*, 11766−11774.
(16) Caboi, F.; Nylander, T.; Razumas, V.; Talaikytë, Z.; Monduzzi, M.; Larsson, K. *Langmuir* **1997**, *13*, 5476−5483.
(17) Razumas, V.; Talaikytë, Z.; Barauskas, J.; Nylander, T.; Miezis, Y. *Prog. Colloid Polym. Sci.* **1998**, *108*, 76−82.
(18) Barauskas, J.; Razumas, V.; Nylander, T. *Prog. Colloid Polym. Sci.* **2000**, *116*, 16−20.
(19) Rowinski, P.; Bilewicz, R.; Stebe, M.-J.; Rogalska, E. *Anal. Chem.* **2002**, *74*, 1554−1559.
(20) Barauskas, J.; Razumas, V.; Talaikytë, Z.; Bulovas, A.; Nylander, T.; Tauraitë, D.; Butkus, E. *Chem. Phys. Lipids* **2003**, *123*, 87−97.
(21) Rowinski, P.; Bilewicz, R.; Stebe, M.-J.; Rogalska, E. *Anal. Chem.* **2004**, *76*, 283−291.
(22) Amar-Yuli, I.; Garti, N. *Colloids Surf. B* **2005**, *43*, 72−82.
(23) Amar-Yuli, I.; Wachtel, E.; Ben-Shoshan, E.; Danino, D.; Aserin, A.; Garti, N. *Langmuir* **2007**, *23*, 3637−3645.
(24) Nilsson, P. G.; Lindman, B. *J. Phys. Chem.* **1983**, *87*, 4756−4761.
(25) Chidichimo, G.; De Fazio, D.; Ranieri, G. A.; Terenzi, M. *Chem. Phys. Lett.* **1985**, *117*, 514−517.
(26) Chidichimo, G.; Coppola, L.; La Mesa, C.; Ranieri, G. A.; Saupe, A. *Chem. Phys. Lett.* **1988**, *145*, 85−89.
(27) Holmes, M. C.; Sotta, P.; Hendrikx, Y.; Deloche, B. *J. Phys. II* **1993**, *3*, 1735−1746.
(28) Nakano, M.; Sugita, A.; Matsuoka, H.; Handa, T. *Langmuir* **2001**, *17*, 3917−3922.
(29) Caboi, F.; Borné, J.; Nylander, T.; Khan, A.; Svendsen, A.; Patkar, S. *Colloids Surf. B* **2002**, *26*, 159−171.
(30) Håkansson, B.; Hansson, P.; Regev, O.; Söderman, O. *Langmuir* **1998**, *14*, 5730−5739.
(31) Coppola, L.; La Mesa, C.; Ranieri, G. A.; Terenzi, M. *J. Chem. Phys.* **1993**, *98*, 5087−5090.
(32) Fukuda, K.; Olsson, U.; Würz, U. *Langmuir* **1994**, *10*, 3222−3229.
(33) Coppola, L.; Oliviero, C.; Olsson, U.; Ranieri, G. A. *Langmuir* **2000**, *16*, 4180−4184.
(34) Baciu, M.; Olsson, U.; Leaver, M. S.; Holmes, M. C. *J. Chem. Phys.* **2006**, *110*, 20781−20788.
(35) Yethiraj, A.; Capitani, D.; Burlinson, N. E.; Burnell, E. E. *Langmuir* **2005**, *21*, 3311−3321.
(36) Feiweier, T.; Heil, B.; Pospiech, E. V.; Fujara, F.; Winter, R. *Phys. Rev. E* **2000**, *62*, 8182−8194.
(37) Liu, L.; John, V. T.; McPherson, G.; Maskos, K.; Bose, A. *Langmuir* **2005**, *21*, 3795−3801.
(38) Amenitsch, H.; Edlund, H.; Khan, A.; Marques, E. F.; Mesa, C. L. *Colloids Surf. A* **2003**, *213*, 79−92.
(39) Inoue, T.; Matsuda, M.; Nibu, Y.; Misono, Y.; Suzuki, M. *Langmuir* **2001**, *17*, 1833−1840.
(40) Snyder, R. G.; Strauss, H. L.; Elllger, C. A. *J. Phys. Chem.* **1982**, *86*, 5145−5150.
(41) Wartewig, S.; Neubert, R.; Rettig, W.; Hesse, K. *Chem. Phys. Lipids* **1998**, *91*, 145−152.
(42) Nilsson, A.; Holmgren, A.; Lindblom, G. *Chem. Phys. Lipids* **1994**, *71*, 119−131.
(43) Lake, J. A. *Acta Crystallogr.* **1967**, *23*, 191−194.
(44) Landh, T. *J. Phys. Chem.* **1994**, *98*, 8453−8467.
(45) Popescu, G.; Barauskas, J.; Nylander, T.; Tiberg, F. *Langmuir* **2007**, *23*, 496−503.
(46) Lindblom, G.; Larsson, K.; Johansson, L.; Fontell, K.; Forsén, S. *J. Am. Chem. Soc.* **1979**, *101*, 5465−5470.

(47) Borné, J.; Nylander, T.; Khan, A. *Langmuir* **2000**, *16*, 10044−10054.
(48) Glasel, J. A. In *Water: A Comprehensive Treatise*; Franks, F., Ed.; Plenum Press: New York, 1972; Vol. 1, p 215.
(49) Zeng, X.; Liu, Y.; Imperor-Clerc, M. *J. Phys. Chem. B* **2007**, *111*, 5174−5179.
(50) Rand, R. P.; Fuller, N. L. *Biophys. J.* **1994**, *66*, 2127−2138.
(51) Razumas, V.; Larsson, K.; Miezis, Y.; Nylander, T. *J. Phys. Chem.* **1996**, *100*, 11766−11774.
(52) Nilsson, A.; Holmgren, A.; Lindblom, G. *Biochemistry* **1991**, *30*, 2126−2133.
(53) Hübner, W.; Mantsch, H. H. *Biophys. J.* **1991**, *59*, 1261−1272.